Geometric quantum gates in liquid-state NMR based on a cancellation of dynamical phases

Yukihiro Ota,[1,*] Yoshito Goto,[2] Yasushi Kondo,[1,3] and Mikio Nakahara[1,3]
[1]*Research Center for Quantum Computing, Interdisciplinary Graduate School of Science and Engineering, Kinki University, 3-4-1 Kowakae, Higashi-Osaka 577-8502, Japan*
[2]*Interdisciplinary Graduate School of Science and Engineering, Kinki University, 3-4-1 Kowakae, Higashi-Osaka 577-8502, Japan*
[3]*Department of Physics, Kinki University, 3-4-1 Kowakae, Higashi-Osaka 577-8502, Japan*
(Received 7 June 2009; published 10 November 2009)

A proposal for applying nonadiabatic geometric phases to quantum computing, called double-loop method [S.-L. Zhu and Z. D. Wang, Phys. Rev. A **67**, 022319 (2003)], is demonstrated in a liquid-state nuclear magnetic-resonance quantum computer. Using a spin-echo technique, the original method is modified so that quantum gates are implemented in a standard high-precision nuclear magnetic-resonance system for chemical analysis. We show that a dynamical phase is successfully eliminated and a one-qubit quantum gate is realized although the gate fidelity is not high.

DOI: 10.1103/PhysRevA.80.052311 PACS number(s): 03.67.Lx, 03.65.Vf

I. INTRODUCTION

Precise and reliable control of a quantum system is an attractive and challenging experimental issue in quantum physics. In particular, the importance of its application to quantum information processing has been increasing recently. A promising way to achieve this is to employ geometric phases (or, more generally, non-Abelian holonomies) [1,2] because geometric phases are expected to be robust against noise and decoherence under a proper condition [3,4]. A large number of studies for applying their potential robustness to quantum computing have been done, e.g., phase-shift gates with Berry phases [5], nonadiabatic geometric quantum gates [6–13], holonomic quantum computing [14–21], quantum gates with noncyclic geometric phases [22], and so on.

For physical realization of geometric quantum gates, elimination of a dynamical phase is a key point. Jones *et al.* [5] implemented a controlled phase-shift gate with a Berry phase [23,24] by quasistatistically, or slowly, controlling an effective field in a rotating frame. They nulled dynamical phase effects using a conventional spin-echo approach [25]. Zhu and Wang [8] proposed a geometric quantum gate based on the Aharonov-Anandan phase [26,27], which should be fast since a nonadiabatic process is employed. In their proposal, elimination of a dynamical phase is achieved by a double-loop method, where a dynamical phase cancels out while a geometric phase accumulates along two loops.

Although several experimental techniques for the application of geometric phases to quantum computation are available [11–13], explicit implementations of geometric phase gates have not been extensively studied so far. Without explicit implementations, the often-cited advantage of the holonomic quantum gates is nothing more than a desk plan. Thus, such explicit examples are highly desirable. In this paper, we combine Zhu and Wang's approach with Jones *et al.*'s one, employing an Aharonov-Anandan phase for fast gate operation and a spin-echo technique for dynamical phase cancellation, and demonstrate one-qubit gates with a commercial liquid-state nuclear magnetic-resonance (NMR) system. In many experiments of nonadiabatic geometric quantum gates [11–13], the gate operations in which the dynamical phase is arranged to vanish [4,28] have been adopted. In the present paper, we show that we may have another option for physical realization of geometric quantum gates.

The next section summarizes Zhu and Wang's theoretical proposal and our modifications for practical implementation in liquid-state NMR quantum computer. In Sec. III we describe details of our experiments, where implemented gates are evaluated by performing quantum process tomography. Sec. IV is devoted to summary.

II. THEORY

A. Quantum gates with orthonormal cyclic vectors

The Aharonov-Anandan phase is a geometric phase associated with nonadiabatic cyclic time evolution of a quantum system [26,27]. Let us write a state at $t(0 \le t \le \tau)$ as $|\psi(t)\rangle$ in the Hilbert space $\mathcal{H}$ with dimension n. The time evolution of a system is given by the Schrödinger equation with a time-dependent Hamiltonian $H(t)$. We take the natural unit in which $\hbar = 1$. The nonadiabatic cyclic time evolution of the quantum system means that

$$|\psi(\tau)\rangle = U(\tau)|\psi(0)\rangle = e^{i\gamma}|\psi(0)\rangle,$$

where $U(\tau)$ is the time evolution operator and $\gamma \in \mathbb{R}$. Let us call $|\psi(0)\rangle$ a cyclic vector [26]. We note that the dynamical phase γ_{d} associated with this time evolution is

$$\gamma_{\mathrm{d}} = -\int_0^\tau \langle\psi(t)|H(t)|\psi(t)\rangle dt, \tag{1}$$

while the geometric component is defined as

$$\gamma_{\mathrm{g}} = \gamma - \gamma_{\mathrm{d}}.$$

We take a set of orthonormal cyclic vectors, $\{|u_k(0)\rangle\}$ so that

*Present address: CCSE, Japan Atomic Energy Agency, 6-9-3 Higashi-Ueno, Tokyo 110-0015, Japan and CREST(JST), 4-1-8 Honcho, Kawaguchi, Saitama, 332-0012, Japan.

$$|u_k(\tau)\rangle = e^{i\gamma_k}|u_k(0)\rangle,$$

where $k=1,\ldots,n$. Hereafter, we write $|u_k(0)\rangle$ as $|u_k\rangle$ for brevity. A general state $|\Psi(0)\rangle \in \mathcal{H}$ is expressed as $|\Psi(0)\rangle=\Sigma_{k=1}^{n} a_k|u_k\rangle$. Then, we have $|\Psi(\tau)\rangle=U(\tau)|\Psi(0)\rangle = \Sigma_{k=1}^{n} a_k e^{i\gamma_k}|u_k\rangle$. We denote a fixed basis in $\mathcal{H}$ as $\{|l\rangle\}$, which corresponds to the computational basis $\{|0\rangle,|1\rangle\}$ for the case $n=2$. In terms of $\{|l\rangle\}$, we have $|\Psi(\tau)\rangle=\Sigma_{l=0}^{n-1} c_l(\tau)|l\rangle$. It means that $a_k=\langle u_k|\Psi(0)\rangle=\Sigma_{l=0}^{n-1} c_l\langle u_k|l\rangle$, where $c_l=c_l(0)$. Therefore, we find that

$$c_l(\tau) = \sum_{l'=0}^{n-1}\sum_{k=1}^{n} e^{i\gamma_k}\langle l|u_k\rangle\langle u_k|l'\rangle c_{l'} = \sum_{l'=0}^{n-1} V_{ll'}c_{l'}, \tag{2}$$

where

$$V_{ll'} = \sum_{k=1}^{n} e^{i\gamma_k}\langle l|u_k\rangle\langle u_k|l'\rangle. \tag{3}$$

We have $\gamma_k=\gamma_{k,\mathrm{d}}+\gamma_{k,\mathrm{g}}$, where $\gamma_{k,\mathrm{d}}$ and $\gamma_{k,\mathrm{g}}$ are the dynamical and the geometric phases associated with $|u_k\rangle$, respectively.

B. Single-qubit case

Let us consider a single-qubit system. We choose the Hamiltonian $H_1(t)$ as

$$H_1(t) = -\frac{1}{2}\mathbf{\Omega}(t)\cdot\boldsymbol{\sigma},$$

with NMR in mind, where $\boldsymbol{\sigma}=(\sigma_x,\sigma_y,\sigma_z)$ and

$$\mathbf{\Omega}(t) = (\omega_1\cos(\omega_{\mathrm{rf}}t-\phi), -\omega_1\sin(\omega_{\mathrm{rf}}t-\phi), \omega_0). \tag{4}$$

We note that $\mathbf{\Omega}(t)$ is a time-dependent parameter corresponding to the external field and σ_α ($\alpha=x,y,z$) is the αth component of the Pauli matrices. One can freely control ω_0 by taking a proper rotating frame. The transformation to the rotating frame with the frequency ω_{rf} is made possible by the unitary transformation $U=e^{i\omega_{\mathrm{rf}}\sigma_z t/2}$ and the Hamiltonian in the rotating frame is

$$H_{1\mathrm{r}} = U^\dagger H_1 U - iU^\dagger\frac{d}{dt}U = -\frac{1}{2}\Omega\boldsymbol{m}\cdot\boldsymbol{\sigma}, \tag{5}$$

where $\Omega=(\omega_1^2+\Delta^2)^{1/2}$, $\Delta=\omega_0-\omega_{\mathrm{rf}}$, $\boldsymbol{m}=(\sin\chi\cos\phi, \sin\chi\sin\phi, \cos\chi)$, and $\tan\chi=\omega_1/\Delta$. The solution of the Schödinger equation is

$$|\psi(t)\rangle = e^{i\omega_{\mathrm{rf}}t\sigma_z/2}e^{i\Omega t\boldsymbol{m}\cdot\boldsymbol{\sigma}/2}|\psi(0)\rangle. \tag{6}$$

We denote the eigenstates of $\boldsymbol{m}\cdot\boldsymbol{\sigma}$ with eigenvalues ±1 as $|\psi_\pm\rangle$. Their explicit forms are

$$|\psi_+\rangle = e^{-i\phi/2}\cos\frac{\chi}{2}|0\rangle + e^{i\phi/2}\sin\frac{\chi}{2}|1\rangle,$$

$$|\psi_-\rangle = -e^{-i\phi/2}\sin\frac{\chi}{2}|0\rangle + e^{i\phi/2}\cos\frac{\chi}{2}|1\rangle,$$

where $|0\rangle$ and $|1\rangle$ are the eigenstates of σ_z with eigenvalues $+1$ and -1, respectively, and taken as the computational basis. The corresponding Bloch vectors of $|\psi_\pm\rangle$ are

$$\langle\psi_\pm|\boldsymbol{\sigma}|\psi_\pm\rangle = \pm\boldsymbol{m}.$$

We require that $|\psi_\pm\rangle$ be cyclic vectors. Since $|\psi_+\rangle$ and $|\psi_-\rangle$ are mutually orthogonal, they are identified as $\{|u_k\rangle\}$ in Sec. II A. It follows from Eq. (6) that the execution time τ must satisfy the condition $|\omega_{\mathrm{rf}}|\tau/2=\pi$, i.e., $\tau=2\pi/|\omega_{\mathrm{rf}}|$. Then, $|\psi_\pm(\tau)\rangle$ is written as

$$|\psi_\pm(\tau)\rangle = e^{i\gamma_\pm}|\psi_\pm\rangle,$$

where $\gamma_\pm=\pi\pm\pi\Omega/|\omega_{\mathrm{rf}}|$. Figure 1 shows an example of $\mathbf{\Omega}(t)$ and the closed trajectory on the Bloch sphere corresponding to $|\psi_+\rangle$. Using Eq. (1), we find that the dynamical phase is

$$\gamma_{\pm,\mathrm{d}} = \pm\frac{\tau}{2}(\omega_1\sin\chi+\omega_0\cos\chi) = \pm\frac{\pi(\omega_1^2+\omega_0\Delta)}{|\omega_{\mathrm{rf}}|\Omega},$$

while the geometric phase is

$$\gamma_{\pm,\mathrm{g}} = \gamma_\pm - \gamma_{\pm,\mathrm{d}} = \pi\left(1\mp\frac{\omega_{\mathrm{rf}}}{|\omega_{\mathrm{rf}}|}\frac{\Delta}{\Omega}\right).$$

Based on Eqs. (2) and (3), we obtain a unitary gate with the dynamical and the Aharonov-Anandan phases with respect to the computational basis $\{|0\rangle,|1\rangle\}$,

$$V(\tau) = \begin{pmatrix} \cos\gamma - i\sin\gamma\cos\chi & -ie^{-i\phi}\sin\gamma\sin\chi \\ -ie^{i\phi}\sin\gamma\sin\chi & \cos\gamma + i\sin\gamma\cos\chi \end{pmatrix},$$

where $\gamma=2\pi-\gamma_+=\gamma_-$ has been used to simplify the notation.

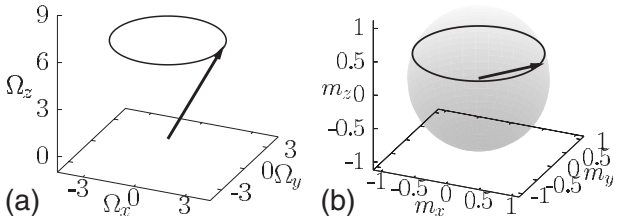

FIG. 1. Example of dynamics of a single-qubit cyclic vector. (a) A time-dependent external field $\mathbf{\Omega}(t)$ and (b) a closed trajectory on the Bloch sphere corresponding to a cyclic vector $|\psi_+(t)\rangle$, $0\le t\le\tau=2\pi/|\omega_{\mathrm{rf}}|$. The end point of each arrow represents the initial value. We set the parameters $\omega_0=2\pi$, $\omega_1=0.5\times2\pi$, $\omega_{\mathrm{rf}}=0.8\times2\pi$, and $\phi=0$ in Eq. (4).

C. Cancellation of dynamical phases

We closely follow Zhu and Wang's proposal [8] in order to eliminate a dynamical phase. They proposed the use of two successive unitary operations, in which a dynamical phase cancels out while a geometric phase accumulates along these two operations. Each unitary operation associated with a loop is characterized by time-dependent external field (4). The loop parameter corresponding to the ith loop is denoted by $\mathbf{\Omega}_i(t)$ ($i=1,2$). Thus, in principle, we have four independent parameters in each loop, i.e., $\omega_{i,1}$, $\omega_{i,\mathrm{rf}}$, ϕ_i, and $\omega_{i,0}$. We note that they are not always tunable in a real experimental situation.

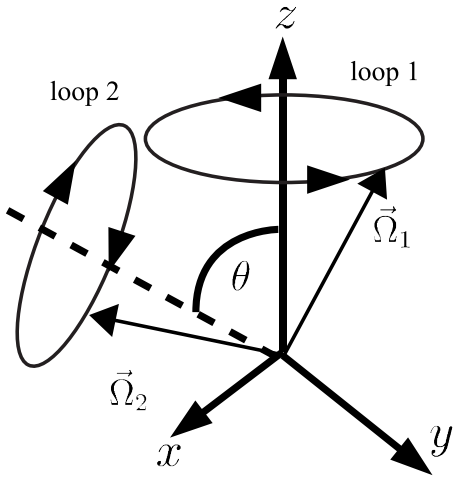

FIG. 2. Schematic diagram of double-loop method for dynamical phase cancellation according to the proposal by Zhu and Wang [8]. Two time-dependent magnetic fields are applied sequentially. The first magnetic field (loop 1) rotates counterclockwise, while the second one (loop 2) rotates clockwise in order to eliminate a dynamical phase.

We will search for the condition under which the dynamical phases associated with the two loops cancel each other as shown in Fig. 2. We focus on the case in which $\phi_i=0$ and $\omega_{1,\mathrm{rf}}=\omega_{2,\mathrm{rf}}(\equiv\omega_{\mathrm{rf}})>0$ for simplicity. The first loop (loop 1) is described by

$$\mathbf{\Omega}_1(t)=(\omega_{1,1}\cos\omega_{\mathrm{rf}}t,-\omega_{1,1}\sin\omega_{\mathrm{rf}}t,\omega_{1,0}), \tag{7}$$

while the second loop (loop 2) by

$$\mathbf{\Omega}_2(t)=-(\omega_{2,1}\cos\omega_{\mathrm{rf}}t,-\omega_{2,1}\sin\omega_{\mathrm{rf}}t,\omega_{2,0})\boldsymbol{R}_y(\theta). \tag{8}$$

Let $\boldsymbol{R}_y(\theta)\in\mathrm{SO}(3)$ represent a rotation around the y-axis by an angle θ. The rotation angle θ is chosen so that the corresponding cyclic vectors $|\psi_{i,\pm}\rangle$ for these two loops satisfies

$$|\psi_{1,\pm}\rangle=e^{ic}|\psi_{2,\pm}\rangle, \tag{9}$$

where $c\in\mathbb{R}$. In other words, the Bloch vectors corresponding to $|\psi_{1,\pm}\rangle$ coincide with those to $|\psi_{2,\pm}\rangle$. Using the notation in Eq. (5), we find that in the loop i

$$\boldsymbol{m}_i=\boldsymbol{k}_i\boldsymbol{O}_i,\quad \boldsymbol{k}_i=(\sin\chi_i,0,\cos\chi_i),$$

where $\boldsymbol{O}_1=\boldsymbol{I}_3$, $\boldsymbol{O}_2=\boldsymbol{R}_y(\theta)$, and we write the 3×3 unit matrix as $\boldsymbol{I}_3$. The rotation angle χ_i is defined as

$$\tan\chi_1=\frac{\omega_{1,1}}{\Delta_1},\quad \Delta_1=\omega_{1,0}-\omega_{\mathrm{rf}}, \tag{10}$$

$$\tan\chi_2=\frac{\omega_{2,1}}{\Delta_2},\quad \Delta_2=\omega_{2,0}+\omega_{\mathrm{rf}}. \tag{11}$$

The angle θ is explicitly given as

$$\theta=\chi_2-\chi_1.$$

Figure 3(a) shows an example of the time-dependent external fields $\mathbf{\Omega}_1(t)$ and $\mathbf{\Omega}_2(t)$. The corresponding closed trajectory on the Bloch sphere is drawn in Fig. 3(b), in which the initial point corresponds to a cyclic vector $|\psi_{1,+}\rangle$. Figure 3(b) shows that $|\psi_{1,+}\rangle$ is not only cyclic for loop 1 but also for the total process (i.e., loop 1 and loop 2) due to connection condition (9). It is necessary to search for $\omega_{i,a}$ and $\omega_{\mathrm{rf}}(a=0,1)$ so that

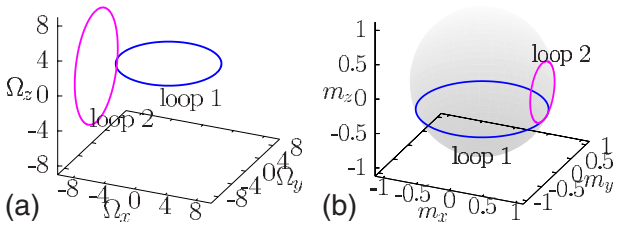

FIG. 3. (Color online) Example of Zhu-Wang's double-loop method. The time-dependent external fields $\mathbf{\Omega}_1(t)$ and $\mathbf{\Omega}_2(t)$ are shown in (a), while the closed trajectory on the Bloch sphere corresponding to the cyclic vectors $|\psi_{1,+}\rangle$ and $|\psi_{2,+}\rangle$ in (b). We note that these are connected and thus form one closed trajectory. We set the loop parameters $\omega_{1,1}=\omega_{2,1}=2\pi$, $\omega_{\mathrm{rf}}=0.7\times2\pi$, $\omega_{1,0}=0.27\times2\pi$, and $\omega_{2,0}=1.5\times2\pi$ in Eqs. (7) and (8). We note that these parameters are calculated on the basis of a condition for nulling dynamical phases in Ref. [8]. In this example, $\Gamma=\frac{1}{2}$ in Eq. (13).

$$\gamma_{1,\mathrm{d}}+\gamma_{2,\mathrm{d}}=0, \tag{12}$$

$$\gamma_{1,\mathrm{g}}+\gamma_{2,\mathrm{g}}=\Gamma\pi. \tag{13}$$

We write them more explicitly as follows:

$$\frac{\omega_{1,1}^2+\omega_{1,0}\Delta_1}{\Omega_1}=\frac{\omega_{2,1}^2+\omega_{2,0}\Delta_2}{\Omega_2}, \tag{14}$$

$$\frac{\Delta_1}{\Omega_1}+\frac{\Delta_2}{\Omega_2}=2-\Gamma, \tag{15}$$

where $\Omega_i=(\omega_{i,1}^2+\Delta_i^2)^{1/2}$. There may be many combinations of $\omega_{i,a}$ and ω_{rf} for a given Γ which satisfy conditions (14) and (15) [8]. We note that a set of the parameters employed in Fig. 3 is one example for the solution of Eqs. (14) and (15), in which $\Gamma=\frac{1}{2}$.

After the elimination of a dynamical phase, we have a one-qubit geometric quantum gate

$$V_{\mathrm{ZW}}=e^{i\Gamma\pi}|\psi_{1,+}\rangle\langle\psi_{1,+}|+e^{-i\Gamma\pi}|\psi_{1,-}\rangle\langle\psi_{1,-}|. \tag{16}$$

D. Spin-echo approach

Zhu and Wang's proposal for eliminating a dynamical phase is not feasible for a conventional commercial NMR system where a field along the z axis is strictly constant. In other words, it is difficult to realize $\mathbf{\Omega}_2(t)$ in Eq. (8). In the present paper, we propose an experimentally feasible method, in which the loop 2 is divided into three successive steps while the loop 1 remains unchanged. The separation of the loop 2 is motivated by the spin-echo technique frequently employed in NMR experiments, in which the direction of time is reversed by an application of a pair of π pulses. Three successive operations are (a) a rotation around the y axis by $\theta(=\chi_2-\chi_1)$, (b) an operation corresponding to precession by a field $-(\omega_{2,1}\cos\omega_{\mathrm{rf}}t,\omega_{2,1}\sin\omega_{\mathrm{rf}}t,\omega_{2,0})$ for a du-

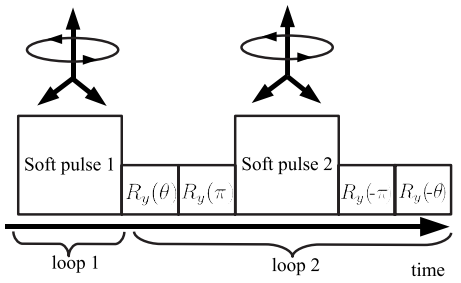

FIG. 4. Schematic diagram of double-loop method for dynamical phase cancellation on the basis of a spin-echo approach. Two (four) soft (hard) square pulses are applied. We note that $R_y(\theta)=e^{-i\theta\sigma_y/2}$, in which $\theta=\chi_2-\chi_1$.

ration $\tau=2\pi/|\omega_{\rm rf}|$, and (c) a rotation around the y axis by $-\theta$. The rotations $R_y(\pm\theta)$ correspond to the basis vector change and back as shown in Fig. 4. Rotation around the y axis by θ is easy to realize by a radio-frequency (rf) pulse, which corresponds to the unitary operator

$$R_y(\theta)=e^{-i\theta\sigma_y/2}. \tag{17}$$

We emphasize here that $|\psi_{2,\pm}\rangle=R_y(\theta)|\psi_{1,\pm}\rangle$. We assume that the pulse duration is infinitely short for simplicity. It should be noted that this operation does not generate a dynamical phase since the y axis is perpendicular to both $\boldsymbol{k}_1$ and $\boldsymbol{k}_2$ [4,28]. The operation corresponds to a precession by a field $-(\omega_{2,1}\cos\omega_{\rm rf}t,\omega_{2,1}\sin\omega_{\rm rf}t,\omega_{2,0})$ for $\tau=2\pi/|\omega_{\rm rf}|$ is given as

$$U_2'=e^{i\Omega_2\tau(-\boldsymbol{k}_2)\cdot\boldsymbol{\sigma}/2},$$

from Eq. (6). The identity

$$R_y(-\pi)e^{i\theta\boldsymbol{k}_2\cdot\boldsymbol{\sigma}/2}R_y(\pi)=e^{i\theta(-\boldsymbol{k}_2)\cdot\boldsymbol{\sigma}/2},$$

implies that U_2' can be realized by a precession under the field $(\omega_{2,1}\cos\omega_{\rm rf}t,-\omega_{2,1}\sin\omega_{\rm rf}t,\omega_{2,0})$ for $\tau=2\pi/|\omega_{\rm rf}|$ sandwiched by a pair of $\pm\pi$ pulses [25]. We again assume that $R_y(\pm\pi)$ is implemented for an infinitely short pulse for simplicity.

Summarizing the above arguments, the total process is described by $R_y(-\theta)R_y(-\pi)U_2(\tau)R_y(\pi)R_y(\theta)U_1(\tau)$ [29], which is equivalent to Eq. (16) if the dynamical phase is zero. The unitary operator $U_i(\tau)$ is defined as $U_i(\tau)=e^{i\omega_{\rm rf}\tau\sigma_y/2}e^{i\Omega_i\boldsymbol{k}_i\cdot\boldsymbol{\sigma}/2}$. The geometric gate which we are going to demonstrate takes the form

$$U_{\rm echo}=R_y(-\pi)U_2(\tau)R_y(\pi)R_y(\theta)U_1(\tau). \tag{18}$$

Although the complete realization of Zhu and Wang's original proposal (16) requires $R_y(-\theta)$ at the end of process (18), we can omit it for constructing a geometric quantum gate since $R_y(-\theta)$ does not generate any dynamical phase here. We note that $V_{\rm ZW}=R_y(-\theta)U_{\rm echo}$. Under conditions (12) and (13), the matrix representation of Eq. (18) in the computational basis $\{|0\rangle,|1\rangle\}$ is given by

$$U_{\rm echo}=\begin{pmatrix}\cos(\Gamma\pi)\cos(\theta/2)-i\sin(\Gamma\pi)\cos\Theta & -\cos(\Gamma\pi)\sin(\theta/2)-i\sin(\Gamma\pi)\sin\Theta\\ \cos(\Gamma\pi)\sin(\theta/2)-i\sin(\Gamma\pi)\sin\Theta & \cos(\Gamma\pi)\cos(\theta/2)+i\sin(\Gamma\pi)\cos\Theta\end{pmatrix}, \tag{19}$$

where $\Theta=(\chi_2+\chi_1)/2$. We note that $\Gamma\pi$ is the total geometric phase. Pulse sequence (18) leads to intuitive understanding of the cancellation mechanism of the dynamical phase. Let us consider the case of $\chi_1=\chi_2$, i.e., the two loop are completely identical, for simplicity. If no π pulse is applied, the dynamical property of the loop 1 is the same as that of the loop 2 and the total dynamical phase is the addition between the contributions from the loops 1 and 2. It should be noted here that the $\pm\pi$-pulses induce the time-reversal dynamics in the form of U_2' in the loop 2. Under the time-reversal transformation, the sign of the dynamical phase associated with the loop 2 is inverted and hence the dynamical phase is completely eliminated. It is necessary to employ different processes between the loops 1 and 2 to prevent the cancellation of the geometric phase associated with the two loops. Matrix representation (19) implies that $U_{\rm echo}$ contains three parameters Γ, θ, and Θ. Due to the limitation in the control parameters, it may be difficult to choose them independently in a standard liquid-state NMR. We will show that θ and Θ should be regarded as functions of Γ and ω_1 in Sec. II E, in order to satisfy Eqs. (12) and (13) as shown in Table I. On the other hand, we are still able to use the rf phase ϕ. Thus, we have the necessary number of free parameters to express arbitrary elements of SU(2).

E. Implementation in liquid-state NMR

We implement the double-loop scheme in liquid-state NMR. We take different loop parameterization from that of Zhu and Wang for ease of implementation. We consider the system in a rotating frame defined by $\omega_{\rm ref}$. Hereafter, we will denote an angular frequency x measured with respect to this rotating frame as $\tilde{x}\equiv x-\omega_{\rm ref}$. Thus, one can explicitly under-

TABLE I. Solutions of Eqs. (12) and (13) for $\Gamma=\frac{1}{2}$ and $\epsilon=\omega_1/|\tilde{\omega}_0|=0.5,0.3,0.1$ in the rotating frame so that $\tilde{\omega}_0<0$. We note that $\tau_i|\tilde{\omega}_{i,\rm rf}|=2\pi$, $\theta=\chi_2-\chi_1$, and $\Theta=(\chi_1+\chi_2)/2$.

ϵ	$\tilde{\omega}_{1,\rm rf}/\tilde{\omega}_0$	$\tilde{\omega}_{2,\rm rf}/\tilde{\omega}_0$	θ [rad]	Θ [rad]
0.5	−0.6815	0.7803	−0.7298	−0.639
0.3	−0.8221	1.105	−0.9571	−0.589
0.1	−0.9422	1.609	−1.008	−0.542

stand which quantities are controllable by choosing a proper rotating frame.

We take a common value

$$\tilde{\omega}_0 = \omega_0 - \omega_{\mathrm{ref}} < 0$$

to $\omega_{1,0}$ and $\omega_{2,0}$. The value of $\tilde{\omega}_0$ in the experiment will be explained in Sec. III B. Similarly, we assume that $\omega_{1,1}=\omega_1$ and $\omega_{2,1}=\omega_1$. Instead of these simplification, we allow different values with respect to ω_{rf} between the two loops, i.e., $\omega_{\mathrm{rf}}=\omega_{1,\mathrm{rf}}$ in Eq. (7) and $\omega_{\mathrm{rf}}=\omega_{2,\mathrm{rf}}$ in Eq. (8). These changes do not alter the basic strategy for searching parameters that satisfy $\gamma_{1,\mathrm{d}}+\gamma_{2,\mathrm{d}}=0$ and $\gamma_{1,\mathrm{g}}+\gamma_{2,\mathrm{g}}=\Gamma\pi$. We consider the two loops in the rotating frame in which the frequency is $\tilde{\omega}_{i,\mathrm{rf}}$, the amplitude ω_1, and the duration $\tau_i=2\pi/|\tilde{\omega}_{i,\mathrm{rf}}|$, i.e.,

$$\tilde{\mathbf{\Omega}}_i(t) = (\omega_1 \cos \tilde{\omega}_{i,\mathrm{rf}}t, -\omega_1 \sin \tilde{\omega}_{i,\mathrm{rf}}t, \tilde{\omega}_0) \quad (0 \le t \le \tau_i).$$

The solutions $\tilde{\omega}_{i,\mathrm{rf}}/|\tilde{\omega}_0|$ are numerically obtained for given $\epsilon(\equiv\omega_1/|\tilde{\omega}_0|)$ and Γ.

We summarize our parameter choice. First of all, we adopt a common value to $\omega_{1,0}$ and $\omega_{2,0}$, i.e., $\tilde{\omega}_0$ in the rotating frame defined as the angular frequency ω_{ref}. The value of $\omega_1(=\omega_{1,1}=\omega_{1,2})$ is given by $\omega_1=\epsilon|\tilde{\omega}_0|$, in which ϵ is a positive number. For a given ϵ and an aimed geometric phase Γ, we can numerically find proper $\tilde{\omega}_{i,\mathrm{rf}}$ so that $\gamma_{1,\mathrm{d}}+\gamma_{2,\mathrm{d}}=0$ and $\gamma_{1,\mathrm{g}}+\gamma_{2,\mathrm{g}}=\Gamma\pi$. The results for $\Gamma=\frac{1}{2}$ and $\epsilon=0.5$, 0.3, and 0.1, for example, are shown in Table I. From the observation of Eqs. (10) and (11), the sign of $\tilde{\omega}_{1,\mathrm{rf}}$ should be opposite to the one of $\tilde{\omega}_{2,\mathrm{rf}}$. It should be noted that the parameters given in Table I are compatible with this requirement. The resultant geometric quantum gate is Eq. (19). The values of $\theta(=\chi_2-\chi_1)$ and $\Theta(=(\chi_2+\chi_1)/2)$ are given in Table I.

When $\Gamma=\frac{1}{2}$, Eq. (19) takes the form

$$U_{\mathrm{echo}}(\Theta) = e^{-i\pi\sigma_y/2}e^{i\Omega_2\tau_2\boldsymbol{k}_2\cdot\boldsymbol{\sigma}/2}e^{-i(\theta+\pi)\sigma_y/2}e^{i\Omega_1\tau_1\boldsymbol{k}_1\cdot\boldsymbol{\sigma}/2}$$
$$= e^{-i\pi/2}\begin{pmatrix}\cos\Theta & \sin\Theta\\ \sin\Theta & -\cos\Theta\end{pmatrix}, \tag{20}$$

which we experimentally demonstrate in the next section.

III. EXPERIMENTS

A. Sample and spectrometer

We implement a one-qubit gate described by Eq. (20) with a conventional commercial NMR system. We employed a JEOL ECA-500 NMR spectrometer [30] whose hydrogen Larmor frequency is approximately 500 MHz. ^{13}C nucleus in a 0.6 ml, 0.2M sample of ^{13}C-labeled chloroform (Cambridge Isotope) in *d*-6 acetone is employed as a qubit, while protons are decoupled by a standard decoupling technique, called WALTZ [25]. We have chosen ^{13}C-labeled chloroform for future experiments involving two-qubit gates. The transverse and the longitudinal relaxation times are $T_2\sim0.3$ s and $T_1\sim5$ s, respectively. The longitudinal relaxation time is shorten by adding a small amount of Fe(III) acetylacetonate so that a repetition rate can be increased. T_2 and T_1 without Fe(III) acetylacetonate are $\sim$0.3 s and $\sim$20 s, respectively.

B. Pulse sequence

As we discussed in the previous section, gate (20) can be realized with two rotating magnetic fields and two hard (short) pulses. The rotating fields are effectively obtained by two soft (long) pulses which are rotating with different frequencies $\tilde{\omega}_{i,\mathrm{rf}}=\omega_{i,\mathrm{rf}}-\omega_{\mathrm{ref}}$ $(i=1,2)$ in the rotating frame with frequency ω_{ref}. The first soft pulse (loop 1) is a usual square pulse, while the second soft pulse (loop 2) is a (frequency) shifted laminar square pulse (SLP) [31]. This SLP is employed in order to obtain the same phase ϕ in Eq. (4) for loop 2 as that for loop 1, i.e., $\phi_1=\phi_2$.

We take $|\tilde{\omega}_0|=2\pi\times1000$ rad/s and $\phi_i=0$ throughout the experiments. The condition $\phi_i=0$ is taken for simplicity as mentioned in the beginning of Sec. II C. We independently calibrate the strengths of the soft and hard pulses in order to minimize a nonlinearity error in setting the rf pulse amplitude. The duration t_{hp} of a hard π pulse is set to 21.6 μs throughout the experiments. We ignore t_{hp} in setting the phase of the second soft pulse, which is justified by the fact that $t_{\mathrm{hp}}|\tilde{\omega}_0|\ll2\pi$. The precision of pulse duration control is 100 ns. The durations $t_{i,\mathrm{sp}}$ of two soft pulses are set to

$$t_{i,\mathrm{sp}}|\tilde{\omega}_{i,\mathrm{rf}}| = 2\pi.$$

We demonstrate three different gates with $\epsilon=0.5$, 0.3, and 0.1. We note that the phase of the second hard pulse corresponding to $R_y(-\pi)$ must be adjusted, presumably because the oscillator in the NMR spectrometer is disturbed in generating a SLP. It should be recalled that a SLP employs intensive phase modulation.

C. Results

Implemented gates with $\Gamma=\frac{1}{2}$ are evaluated by performing quantum process tomography [32]. The practical details are explained in Ref. [33]. A quantum process $\mathcal{E}$, such as a gate operation or relaxation process, is

$$\rho \mapsto \mathcal{E}(\rho) = \frac{\sum_k E_k \rho E_k^\dagger}{\sum_k E_k^\dagger E_k}$$

in the operator sum (or Kraus) representation [34,35]. When all E_k's are determined, $\mathcal{E}$ is considered to be identified. This identification is called quantum process tomography.

The Bloch sphere in Fig. 5(a) is mapped under the gate operations to the surfaces in Figs. 5(b)–5(d), which correspond to $\epsilon=0.5$, 0.3 and 0.1, respectively. If the gate operations are perfect, the surfaces are the spheres of unit radius (i.e., the Bloch sphere). The left panel of each row shows the theoretical final state. In the middle panels, the results for the single gate operation are shown. Finally, the right panels are for the two-successive (double) gate operation. The Hadamard gate obtained when $\Theta=-\pi/4$ is, for comparison, shown in the right panel of Fig. 5(a). From these figures, we find that $U_{\mathrm{echo}}(\Theta)$ in Eq. (20) is implemented although it is not perfect.

We numerically evaluated the fidelity of the implemented gate using the entanglement fidelity [33,35] given by

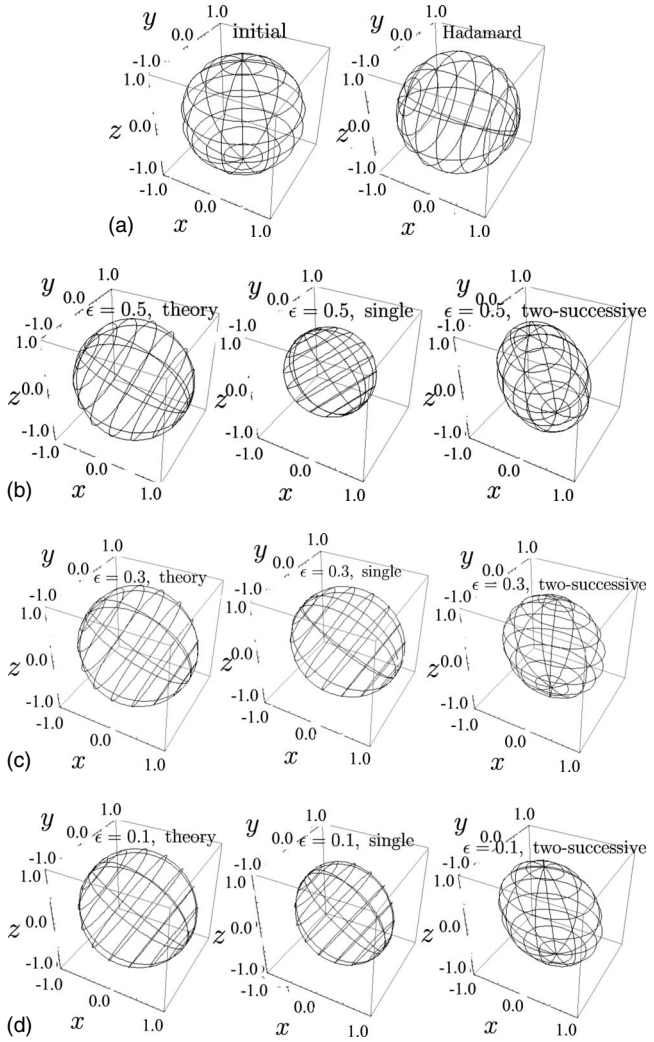

FIG. 5. Gate operations visualized. The Bloch sphere in (a) is mapped to the surfaces in (b)–(d) under the gates with $\epsilon=0.5$, 0.3 and 0.1, respectively. The right surface in (a) is an expected Bloch sphere when $\Theta=-\pi/4$, which corresponds to the Hadamard gate. Each left panel in (b)–(d) corresponds to the theoretical final state. The middle panels are the results for the single gate operation $U_{\text{echo}}(\Theta)$. The right panels are for the two-successive (double) gate operations.

$$F_{\text{e}}(I_0,\mathcal{E}\circ\mathcal{U}_{\text{echo}}^{-1}) = \frac{\sum_k |\text{Tr}[E_k U_{\text{echo}}(-\Theta) I_0]|^2}{\text{Tr}[\sum_k E_k U_{\text{echo}}(-\Theta) I_0 U_{\text{echo}}^{\dagger}(-\Theta) E_k^{\dagger}]}$$

$$= \frac{\sum_k |\text{Tr}[E_k U_{\text{echo}}(-\Theta) I_0]|^2}{\text{Tr}(\sum_k E_k I_0 E_k^{\dagger})},$$

where $\mathcal{U}_{\text{echo}}$ is a super operator corresponding to the unitary operator $U_{\text{echo}}(\Theta)$ [i.e., $\mathcal{U}_{\text{echo}}(\rho)=U_{\text{echo}}(\Theta)\rho U_{\text{echo}}^{\dagger}(\Theta)$], $I_0=\mathbb{1}/2$, and $\mathbb{1}$ is the identity matrix of dimension 2. One can find that $F_{\text{e}}(I_0,\mathcal{E}\circ\mathcal{U}_{\text{echo}}^{-1})=1$ when the gate operation $\mathcal{E}$ is perfect. In the case of two-successive gate operation, $F_{\text{e}}(I_0,\mathcal{E}^2)$ gives a measure of the fidelity since $[U_{\text{echo}}(\Theta)]^2=-\mathbb{1}$. The entanglement fidelities corresponding to the gate operations are summarized in Table II.

TABLE II. The entanglement fidelities for single and double operations with $\epsilon=0.5$, 0.3, and 0.1.

ϵ	$F_{\text{e}}(I_0,\mathcal{E}\circ\mathcal{U}_{\text{echo}}^{-1})$	$\text{Tr}[\mathcal{E}(I_0)]$	$F_{\text{e}}(I_0,\mathcal{E}^2)$	$\text{Tr}[\mathcal{E}^2(I_0)]$
0.5	0.75	1.00	0.74	1.02
0.3	0.88	1.08	0.83	1.07
0.1	0.84	1.07	0.85	1.06

The fidelities of the demonstrated gates are not high. This may be attributed to the inhomogeneous rf field. The free-induction-decay signal of the thermal state after a $5\pi/2$ pulse, which corresponds to the operation $e^{-5\pi\sigma_x/4}$ for example, reduces to about 85% of that after a $\pi/2$ pulse, which corresponds to the operation $e^{-\pi\sigma_x/4}$ for example. This fact indicates that there is some rf field inhomogeneity which may account for most of the reduction in the fidelities in Table II. Pulse sequences in usual NMR operations are designed so that the rf field inhomogeneity does not affect measurements, for example, by employing composite pulses. Such techniques are not available in our experiments.

IV. SUMMARY

We demonstrated the elimination of the dynamical phase and the implementation of the quantum gates with pure nonadiabatic geometric phases in a liquid-state NMR quantum computer, based on the double-loop method. By means of a spin-echo technique, we modified the original proposal so that quantum gates are implemented in a standard high precession NMR system for chemical analysis. We have proposed and experimentally verified an alternative method to eliminate dynamical phase. The extension of the present method to two-qubit operations is an important future work [36]. We believe that our work is the step toward physical realization of working geometric quantum gates and further efforts should be made for improvement of the gates.

ACKNOWLEDGMENTS

This work was supported by "Open Research Center" Project for Private Universities: Matching fund subsidy from MEXT (Ministry of Education, Culture, Sports, Science and Technology). M.N.'s work is supported in part by Grant-in-Aid for Scientific Research (C) from JSPS (Grant No. 19540422).

[1] M. Nakahara, *Geometry, Topology and Physics*, 2nd ed. (CRC Press, Boca Raton, London, New York, 2003).
[2] D. Chruściński and A. Jamiołkowski, *Geometric Phases in Classical and Quantum Mechanics* (Birkhäuser, Boston, 2004).
[3] A. Blais and A.-M. S. Tremblay, Phys. Rev. A **67**, 012308 (2003).
[4] Y. Ota and Y. Kondo, Phys. Rev. A **80**, 024302 (2009).
[5] J. A. Jones, V. Vedral, A. Ekert, and G. Castagnoli, Nature (London) **403**, 869 (2000).
[6] Wang Xiang-Bin and M. Keiji, Phys. Rev. Lett. **87**, 097901 (2001); **88**, 179901(E) (2002).
[7] S. -L. Zhu and Z. D. Wang, Phys. Rev. Lett. **89**, 097902 (2002); **89**, 289901(E) (2002).
[8] S.-L. Zhu and Z. D. Wang, Phys. Rev. A **67**, 022319 (2003).
[9] X.-D. Zhang, S.-L. Zhu, L. Hu, and Z. D. Wang, Phys. Rev. A **71**, 014302 (2005).
[10] S. -L. Zhu and P. Zanardi, Phys. Rev. A **72**, 020301(R) (2005).
[11] M. Tian, Z. W. Barber, J. A. Fischer, and Wm. Randall Babbitt, Phys. Rev. A **69**, 050301(R) (2004).
[12] R. Das, S. K. K. Kumar, and A. Kumar, J. Magn. Reson. **177**, 318 (2005).
[13] H. Imai and A. Morinaga, Phys. Rev. A **76**, 062111 (2007).
[14] P. Zanardi and M. Rasetti, Phys. Lett. A **264**, 94 (1999).
[15] L.-M. Duan, J. I. Cirac, and P. Zoller, Science **292**, 1695 (2001).
[16] A. O. Niskanen, M. Nakahara, and M. M. Salomaa, Phys. Rev. A **67**, 012319 (2003).
[17] P. Solinas, P. Zanardi, and N. Zanghi, Phys. Rev. A **70**, 042316 (2004).
[18] V. Karimipour and N. Majd, Phys. Rev. A **70**, 012320 (2004).
[19] S. Tanimura, M. Nakahara, and D. Hayashi, J. Math. Phys. **46**, 022101 (2005).
[20] H. Goto and K. Ichimura, Phys. Rev. A **75**, 033404 (2007).
[21] Y. Ota, M. Bando, Y. Kondo, and M. Nakahara, Phys. Rev. A **78**, 052315 (2008).
[22] A. Friedenauer and E. Sjöqvist, Phys. Rev. A **67**, 024303 (2003).
[23] M. V. Berry, Proc. R. Soc. London, Ser. A **392**, 45 (1984).
[24] B. Simon, Phys. Rev. Lett. **51**, 2167 (1983).
[25] M. H. Levitt, *Spin Dynamics* (John Wiley & Sons, New York, 2005).
[26] Y. Aharonov and J. Anandan, Phys. Rev. Lett. **58**, 1593 (1987).
[27] D. N. Page, Phys. Rev. A **36**, 3479 (1987).
[28] D. Suter, K. T. Mueller, and A. Pines, Phys. Rev. Lett. **60**, 1218 (1988).
[29] When the rf phases for loops 1 and 2 are not zero, instead of $R_y(\theta)$, one has to perform $e^{-i\phi_2\sigma_z/2}R_y(\theta)e^{i\phi_1\sigma_z}$, where ϕ_i is the rf phase for the loop i. In addition, the π-pulse $R_y(\pi)$ has to be also replaced with $e^{-i\phi_2\sigma_z/2}R_y(\pi)e^{i\phi_2\sigma_z/2}$.
[30] http://www.jeol.com/.
[31] S. L. Patt, J. Magn. Reson. **96**, 94 (1992); see, also, manuals of ECA500 spectrometer provided by JEOL.
[32] I. L. Chuang and M. A. Nielsen, J. Mod. Opt. **44**, 2455 (1997).
[33] Y. Kondo, J. Phys. Soc. Jpn. **76**, 104004 (2007).
[34] K. Kraus, *States, Effects and Operations: Fundamental Notations of Quantum Theory* (Springer-Verlag, Berlin, 1983).
[35] H. Barnum, M. A. Nielsen, and B. Schumacher, Phys. Rev. A **57**, 4153 (1998).
[36] The authors in Ref. [8] claimed that two-qubit gates can be, in principal, realized similarly. In the double-loop method, a connection condition between the two loops, which corresponds to Eq. (9) in the case of one-qubit gates, has to be satisfied. In addition, as for two-qubit gates, the condition for a controlled qubit has to be completely equivalent to the one for a target qubit. We find that Fig. 3 in Ref. [8], on which their two-qubit gate is based, may be erroneous, since this independence condition is not satisfied. We have derived a correct expression, but we can not find the proper parameter sets with which two-qubit gates are implemented.